Cancer Science
Japanese Cancer Association JCA
Open Access

Therapeutic effect of cisplatin given with a lymphatic drug delivery system on false-negative metastatic lymph nodes

Asuka Tada,[1,2,3] Sachiko Horie,[1,2] Shiro Mori[1,2,4] and Tetsuya Kodama[1,2,3]

[1]Laboratory of Biomedical Engineering for Cancer; [2]Biomedical Engineering Cancer Research Center, Graduate School of Biomedical Engineering; [3]Department of Electronic Engineering, Graduate School of Engineering, Tohoku University; [4]Department of Oral and Maxillofacial Surgery, Tohoku University Hospital, Sendai, Japan

Key words

Cisplatin, lymph node metastasis, lymphatic drug delivery system, lymphatic network, MXH10/Mo-*lpr*/*lpr* mouse

Correspondence

Tetsuya Kodama, Laboratory of Biomedical Engineering for Cancer, Graduate School of Biomedical Engineering, Tohoku University, 4-1 Seiryo, Aoba, Sendai, Miyagi 980-8575, Japan.
Tel:/Fax: +81-22-717-7583;
E-mail: kodama@tohoku.ac.jp

Funding Information

Japan Society for the Promotion of Science (JSPS) KAKENHI Grant Numbers 26293425 (S.M.), 16K15816 (S.M.), and 17H00865 (T.K.).

Received April 21, 2017; Revised August 6, 2017; Accepted August 23, 2017

Cancer Sci **108** (2017) 2115–2121

doi: 10.1111/cas.13387

Systemic administration of drugs into the blood circulation is standard treatment for prevention of metastasis. However, systemic delivery cannot maintain sufficiently high concentrations of anticancer drugs in lymph nodes (LN). Here, we show that giving cisplatin (CDDP) using a lymphatic drug delivery system (LDDS) has the potential to treat false-negative metastatic LN. We found that in MXH10/Mo-*lpr*/*lpr* mice, which develop systemic swelling of LN up to 10 mm in diameter, accumulation of indocyanine green (ICG), which has a similar molecular weight to CDDP, in a target LN was greater for lymphatic delivery of ICG than for systemic (i.v.) administration. Furthermore, CDDP administration with a LDDS inhibited tumor growth in false-negative metastatic LN and produced fewer adverse effects than systemically given CDDP. We anticipate that drug delivery using a LDDS will, in time, replace systemic chemotherapy for the treatment of false-negative metastatic LN.

Lymph node metastasis occurs before distant metastasis in many cancers.[1–4] Although LN dissection is effective for LN identified by imaging techniques as containing metastases,[5] resection is invasive and often challenging.[6] Systemic chemotherapy is also used but has limitations such as low selectivity, low drug retention in metastatic LN and serious adverse effects.[7,8] As metastatic LN can be a source of systemic metastasis,[9–11] effective therapies are needed for early-stage LN metastasis. We have established a colony of MXH10/Mo-*lpr*/*lpr* (MXH10/Mo/lpr) inbred mice, which develop systemic swelling of LN that reach up to 10 mm in diameter (similar in size to human LN).[12] Furthermore, we have developed diagnostic[13,14] and therapeutic[9,15–18] methods for the early stage of LN metastasis. We define a LN during the early stage of metastasis as a false-negative LN, because its size at that stage of tumor development is not significantly different from that of a LN not containing tumor cells (i.e. a normal LN).[16,19–21] Anatomical studies in MXH10/Mo/lpr mice have revealed that the PALN and AALN are located in the axillary area and that the PALN is downstream of both the AALN and SiLN.[10] We have provided proof-of-concept for a LDDS that could be used to treat/prevent LN micrometastasis.[9,18] The principle is that a chemotherapeutic drug is injected before surgical resection into an upstream LN (within the dissection area) so that it is delivered at high concentrations to a downstream metastatic LN (outside the dissection area). In the present study, we evaluated the anticancer effect of CDDP delivered to a false-negative LN using a LDDS. In initial experiments, the accumulation of ICG in the PALN (the "target" LN) was compared between injection into the AALN (an "upstream" LN) and systemic administration through the tail vein. Next, tumor cells were inoculated into the SiLN to induce metastasis to the PALN and CDDP was injected into the AALN to investigate its anticancer action in the metastasized PALN.

Materials and Methods

All *in vivo* studies were approved by the Institutional Animal Care and Use Committee of Tohoku University.

Mice. MXH10/Mo/lpr mice[12] were bred at the Institute for Animal Experimentation, Graduate School of Medicine, Tohoku University, Japan. Thirty-five male and female mice were used (weight, 30–42 g; age, 16–18 weeks).

Cell culture. C3H/He mouse mammary carcinoma (FM3A-Luc) cells expressing the luciferase gene[12] were maintained in RPMI-1640 medium (Sigma Chemical Co., St Louis, MO, USA) supplemented with 10% (v/v) FBS (Hyclone, GE

Healthcare UK Ltd, Little Chalfont, UK), 1% (v/v) L-glutamine-penicillin-streptomycin (Sigma) and 1 mg/mL G418 (Wako Pure Chemical Industries, Osaka, Japan). Cells expressed VEGF-A and VEGF-B but not VEGF-C.[14] Cell lines were incubated (37°C, 5% CO_2/95% air) until 80% confluence was achieved. Lack of *Mycoplasma* contamination was confirmed on the inoculation day (MycoAlert *Mycoplasma* Detection Kit; Lonza, Rockland, ME, USA). Relative cell growth rate was 1.1/day.[22]

Biodistribution of ICG after administration systemically or with a LDDS. One hundred and twenty microlitres of 100 μg/mL ICG (molecular weight, 775; excitation wavelength, 774 nm; emission wavelength, 805 nm; Daiichi Sankyo, Osaka, Japan) was injected into the tail vein (IV group; $n = 4$) or AALN (LDDS group; $n = 7$) of mice anesthetized using 2% isoflurane (Abbotto Japan, Chiba, Japan) in O_2. Injection into the AALN was carried out using a 27-G butterfly needle under the guidance of a HFUS imaging system (VEVO770; VisualSonics, Toronto, Canada) using a 25-MHz transducer (RMV-710B; axial resolution, 70 μm; focal length, 15 mm; VisualSonics). Before and 0.5, 2, 6 and 24 h after ICG injection, fluorescence intensity was measured using a biofluorescence imaging system (*in vivo* imaging system; IVIS; Xenogen, Waltham, MA, USA). At 24 h after ICG injection, 1 mL blood was collected from the inferior vena cava, incubated with 10–20 μL of 10% EDTA for 30 min at room temperature and centrifuged (4°C, × 13 000 *g*) for 10 s to obtain plasma. Fluorescence intensities of the plasma samples were measured using IVIS. After blood sample collection, heart, lungs, liver, bilateral kidneys, spleen, PALN and AALN were harvested and weighed. Fluorescence intensity of each organ was measured using IVIS and quantified according to organ weight.

Induction of PALN metastasis by injection of tumor cells into the SiLN. Each mouse was anesthetized with 2% isoflurane in O_2, and the unilateral SiLN was injected (under HFUS guidance) with FM3A-Luc cells (3.3×10^5 cells/mL) suspended in 10 μL PBS plus 20 μL of 400 mg/mL Matrigel (Collaborative Biomedical Products, Bedford, MA, USA). PALN tumor growth was assessed every 3 days post-inoculation through measurements of luciferase activity: 10 min after i.p. injection of luciferin (150 mg/kg; Promega, Madison, WI, USA) under anesthesia (2% isoflurane in O_2), the fluorescence signal from the PALN was measured over a 1-min period using IVIS. PALN metastasis was considered to have occurred when the luciferase activity exceeded the background level in controls (1×10^6 photons/s). The day on which PALN metastasis was confirmed was defined as day -1^T.

Treatment of metastatic PALN with CDDP. Mice with confirmed PALN metastasis were randomly divided into LDDS and IV groups. The LDDS group was further divided into three subgroups ($n = 5$): 0 μg/g CDDP (saline without CDDP), 0.5 μg/g CDDP and 5 μg/g CDDP. For the LDDS subgroups, CDDP (molecular weight, 300; Wako Pure Chemical Industries) in 120 μL saline was injected into the AALN using a 27-G butterfly needle under HFUS guidance. For the IV group, a bolus injection of CDDP (5 μg/g, $n = 5$) was given into the tail vein. Luciferase activity was measured by IVIS at days 3^T, 6^T and 9^T after administration. SiLN, PALN, AALN and lungs were harvested at day 9^T, and luciferase activities of the samples (in six-well plates) were measured by IVIS (0.3 mg/mL luciferin).

Measurement of PALN and AALN volumes. Proper axillary lymph node and AALN volumes were measured using a HFUS imaging system (VEVO770) with a 25-MHz transducer (RMV-710B) on the inoculation day and days 0^T and 9^T.

Blood biochemistry to assess renal/hepatic toxicity. Sixteen mice were assigned to the IV group (5 μg/g CDDP, $n = 3$) and three LDDS groups: 0 μg/g CDDP ($n = 4$), 0.5 μg/g CDDP ($n = 4$) and 5 μg/g CDDP ($n = 5$), respectively. Blood was drawn from the left ventricle at day 9^T (under general anesthesia) and plasma obtained by centrifugation at 13 000 *g* for 10 s. Hepatic and renal functions were evaluated from plasma measurements of T-Bil, ALT, AST, Cre and BUN (Oriental Yeast, Tokyo, Japan).

Histological analysis. Tissues (PALN, AALN and kidney) were excised at day 9^T, fixed overnight in 10% formalin at 4°C, dehydrated, embedded in paraffin, serially sectioned (3–4 μm), and either stained with H&E or immunostained for LYVE-1-positive and CD31-positive cells (Discovery XT Automated Staining Processor; Ventana Medical Systems, Tucson, AZ, USA).[19]

Statistical analysis. Data are presented as mean ± standard deviation (SD). Differences between groups were determined by non-parametric tests (Mann–Whitney *U*-test, Wilcoxon signed rank test or Kruskal-Wallis test with post-hoc test) using GraphPad Prism 6J (GraphPad). $P < 0.05$ was considered statistically significant.

Results

ICG biodistribution. These experiments evaluated drug retention in a LN after administration by a LDDS or i.v. injection. In the LDDS group, the highest fluorescence signal was detected in the axillary area at 2 h post-injection of ICG into the AALN (Fig. 1A), and the accumulated ICG was retained in the axillary area at 24 h post-injection. In the IV group, no fluorescence signal was detected in the axillary area, whereas a notable fluorescence signal was detected in the liver for up to 6 h. Next, *ex vivo* ICG fluorescence intensity was measured in various excised organs and plasma samples 24 h after post-injection of ICG (Fig. 1B). Notable fluorescence signals were detected in the kidneys, liver, PALN and AALN in the LDDS group, but only in the kidneys and liver in the IV group (Fig. 1Ba). Weight-normalized fluorescence intensity (Fig. 1Bb) differed significantly between the LDDS and IV groups for the liver ($P < 0.05$), PALN ($P < 0.05$) and AALN ($P < 0.01$), whereas the plasma fluorescence intensity did not differ between groups (Fig. 1Bc).

Treatment of false-negative metastatic LN using CDDP given by a LDDS. As PALN retention of ICG was higher for the LDDS group than for the IV group (Fig. 1), a similar effect was anticipated for CDDP. Tumor cells were inoculated into the SiLN (day 0) to induce PALN metastasis (Fig. 2Aa–2Ab). Luciferase activity increased with time after inoculation in both the SiLN and PALN (Fig. 2Ab) but was higher in the SiLN (injection site). PALN metastasis was detected at 21 days post-inoculation (Fig. 2Aa).

CDDP was given to metastatic PALN by LDDS or i.v. injection on day 0^T (the day after detection of metastasis). Figure 2Ba and 2Bb shows the treatment effects in the various LDDS and IV groups. Figure 2Bb shows normalized *in vivo* luciferase activity versus days after treatment. Although a significant difference was not observed between each group, among the LDDS groups, PALN luciferase activity was lower in the 5 μg/g CDDP group than in the 0 μg/g CDDP or 0.5 μg/g CDDP groups ($P < 0.05$). The IV group (5 μg/g CDDP) showed no decrease in PALN luciferase activity versus the LDDS 0 μg/g CDDP group. Luciferase activity in the LDDS 5 μg/g CDDP group was highest at day 3^T and then decreased at days 6^T and 9^T. Figure 2Ca shows *ex vivo* bioluminescence images of SiLN,

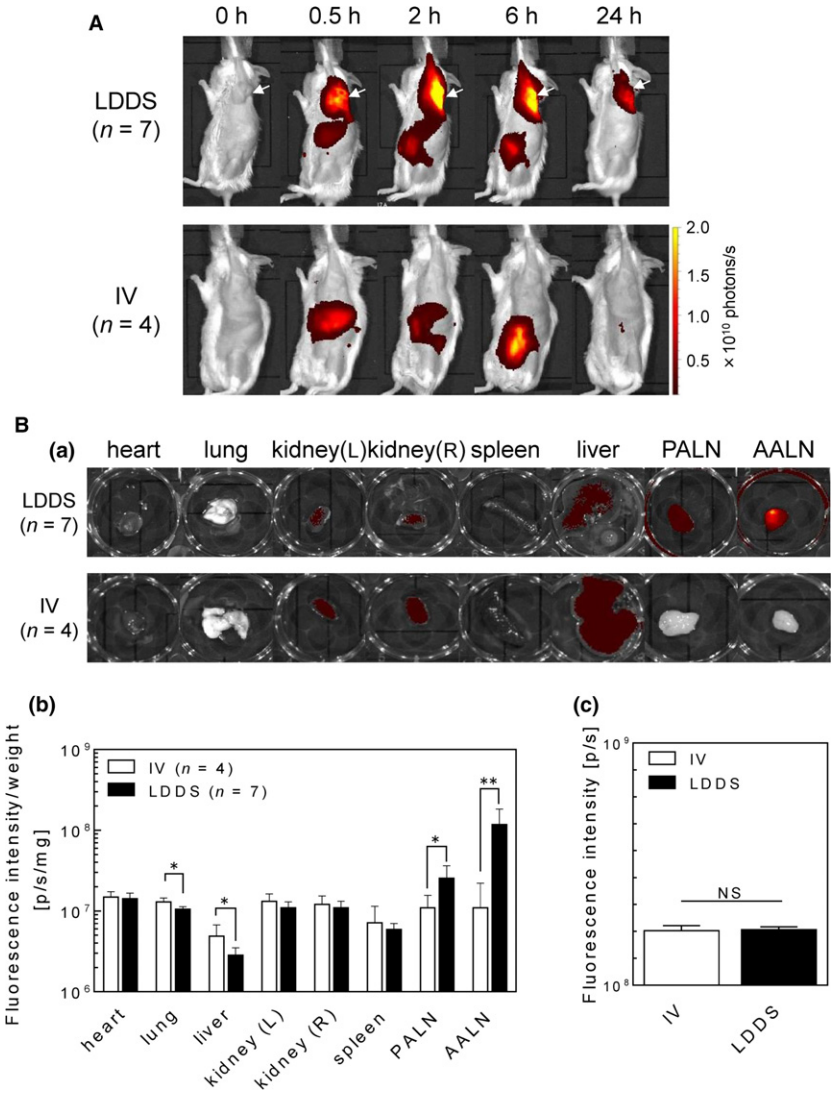

Fig. 1. Biodistribution of indocyanine green (ICG) after systemic administration or lymphatic injection into the accessory axillary lymph node (AALN). (A) *In vivo* whole body fluorescence images to evaluate the distribution of ICG in mice at different time points post-injection. The lymphatic drug delivery system (LDDS) group shows high fluorescence in the axillary area (white arrows) for 24 h after ICG injection. In contrast, fluorescence was not detected in the axillary area in the i.v. injection (IV) group, and ICG seemed to accumulate in the liver. (B) *Ex vivo* fluorescence images at 24 h post-injection of ICG. (a) *Ex vivo* fluorescence images of each organ. For the LDDS group ($n = 7$), ICG fluorescence was detected in the proper axillary lymph node (PALN) and AALN. However, for the IV group ($n = 4$), fluorescence levels in the PALN and AALN were below the limits of detection. (b) *Ex vivo* fluorescence intensity of each organ normalized to its weight. Statistically significant differences between the LDDS and IV groups were found for the liver, PALN and AALN (Mann–Whitney *U*-test: $*P < 0.05$, liver; $*P < 0.05$, PALN; $**P < 0.01$, AALN). (c) *In vitro* fluorescence intensity of plasma. There was no significant difference between the IV ($n = 4$) and LDDS ($n = 4$) groups (Mann–Whitney *U*-test).

PALN, AALN and lung samples, obtained at day 9^T. PALN luciferase activity was detected in the LDDS 0 μg/g CDDP, LDDS 0.5 μg/g CDDP and IV (5 μg/g CDDP) groups but not in the LDDS 5 μg/g CDDP group. Luciferase signals in the AALN or lung were not detected in any of the groups. Figure 2Cb shows *ex vivo* luciferase activity in the SiLN, PALN, AALN and lung (day 9^T). For the PALN, there were significant differences between the LDDS 0 μg/g CDDP and LDDS 5 μg/g CDDP groups ($P < 0.05$).

Changes in PALN volume (assessed using HFUS imaging) were used to evaluate the antitumor effect of CDDP. Figure 3Aa shows representative images of a PALN at day 9^T. For all groups, PALN volume changes were not detected between the inoculation day and day 0^T (Fig. 3Ab). At day 9^T, the largest PALN volume was observed in the LDDS 0 μg/g CDDP group; the PALN volume increase was likely because of tumor growth. PALN volume on day 9^T was significantly smaller in the LDDS 5 μg/g CDDP group than in the LDDS 0 μg/g CDDP group, indicating that tumor growth had been inhibited ($P < 0.05$; Fig. 3Ac). AALN volume at day 9^T was significantly decreased in the LDDS 5 μg/g CDDP and IV (5 μg/g CDDP) groups compared with the LDDS 0 μg/g CDDP group ($P < 0.001$ and $P < 0.01$, respectively).

Blood biochemistry and animal weight. To determine whether use of LDDS was associated with toxicity, blood biochemical parameters at day 9^T and changes in animal weight during the study were assessed. There were no statistically significant differences between the four groups (Table 1).

Histological analysis. Figure 4 shows representative sections stained at day 9^T with H&E, anti-CD31 antibody or anti-LYVE-1 antibody. In all groups, lymphatic vessels were expanded by tumor growth (Fig. 4A3, 4B3, 4C3, 4D3). In the LDDS 0 μg/g CDDP, LDDS 0.5 μg/g CDDP and IV groups, tumor cells were widely distributed in the PALN (Fig. 4A1–4A3, 4B1–4B3, 4C1–4C3, 4D1–4D3). In the LDDS 5 μg/g CDDP group (Fig. 4C1–4C3), tumor cells were observed only within lymphatic vessels and not outside them. In sections of the kidneys (Fig. 4A4, 4B4, 4C4, 4D4), proximal tubular atrophy was observed in the IV (5 μg/g CDDP) group but not in any of the LDDS groups.

Discussion

This is the first study to quantify treatment efficacy of a chemotherapy agent given by a LDDS to a false-negative metastatic LN. PALN metastasis, induced by tumor cell

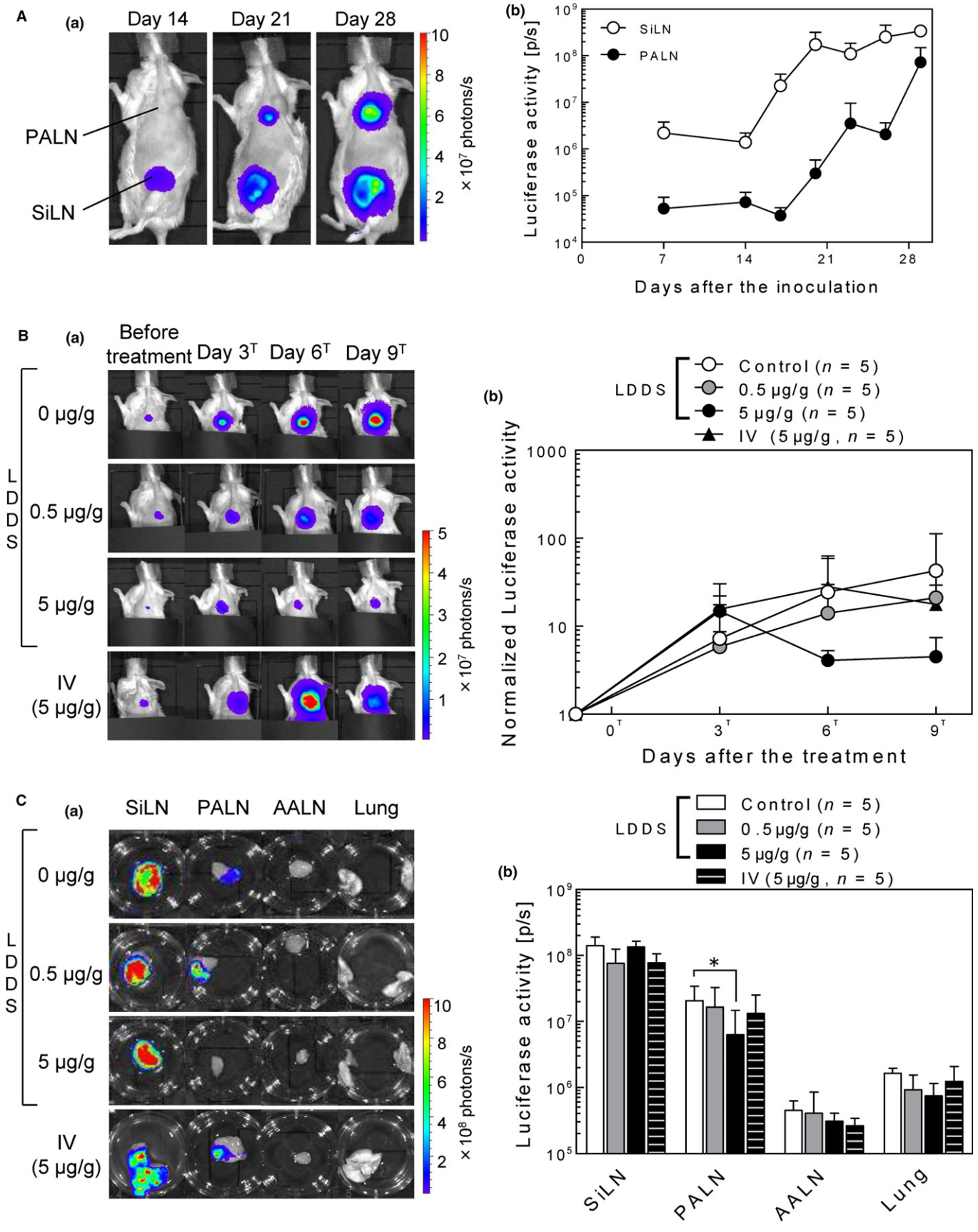

Fig. 2. Antitumor effect of cisplatin (CDDP) in the metastatic proper axillary lymph node (PALN). (A) Induction of metastasis in the PALN. Tumor cells were injected into the subiliac lymph node (SiLN) to induce metastasis to the PALN by lymphatic vessels. (a) *In vivo* bioluminescence imaging. Luciferase activity in the PALN was measured at days 7 and 14 and every 3 days after day 14. Metastasis was considered to have been successfully induced when PALN luciferase activity exceeded the background level of controls (1×10^6 photons/s). (b) Luciferase activity increased with time in both the SiLN (n = 3, 3, 3, 7, 7, 5, 2 for days 7, 14, 17, 20, 23, 26, 29, respectively) and PALN (n = 3, 7, 3, 7, 7, 3, 3 for days 7, 14, 17, 20, 23, 26, 29, respectively), but was higher in the SiLN. (B) *In vivo* bioluminescence imaging after treatment intervention. (a) *In vivo* bioluminescence imaging. The day on which PALN luciferase activity reached 1×10^6 photons/s was defined as day -1^T, and treatment was given on the following day (day 0^T). Mice were divided into lymphatic drug delivery system (LDDS) and i.v. injection (IV) groups, and the LDDS group was subdivided into three groups: 0 μg/g CDDP (saline alone, n = 5), 0.5 μg/g CDDP (n = 5) and 5 μg/g CDDP (n = 5). For the IV group, 5 μg/g CDDP was injected into the tail vein (n = 5). Among the various treatment groups, the LDDS 5 μg/g CDDP group showed the highest inhibition of tumor growth in the PALN. (b) Changes in luciferase activity in PALN. *In vivo* luciferase activity after treatment, normalized in each group to the value at day -1^T. Each group, n = 5. There was no statistical significance between each group on days 3^T, 6^T and 9^T (Kruskal-Wallis test). (C) *Ex vivo* bioluminescence imaging at day 9^T after treatment. (a) Each organ was harvested at day 9^T after treatment and luciferase activity measured. There was no detectable luciferase activity in PALN in the LDDS 5 μg/g CDDP group. There was no detectable luciferase activity in accessory axillary lymph node (AALN) or lungs in all groups. (b) *Ex vivo* luciferase activity at day 9^T after treatment. Each group, n = 5. Kruskal-Wallis test, PALN: $^*P < 0.05$, LDDS 0 μg/g CDDP *vs* LDDS 5 μg/g CDDP.

injection into the SiLN, was treated by injection of CDDP into the AALN (an upstream LN).[9]

First, we gave ICG into the AALN with the LDDS and evaluated ICG accumulation in the PALN (Fig. 1). It was assumed that CDDP would show similar flux/accumulation properties to ICG, as their molecular weights are relatively similar (i.e. CDDP: molecular weight, 300; ICG: molecular weight, 775). Signals in the axillary area were detected 24 h after ICG injection with the LDDS. *Ex vivo* measurements made at 24 h after ICG administration showed that fluorescence intensities in PALN and AALN were higher in the LDDS group than in the IV group (Fig. 1Bb). However, the LDDS group showed less hepatic accumulation of ICG than the IV group (Fig. 1Bb). Second, we investigated the anticancer effects of CDDP on a false-negative metastatic LN. *In vivo* bioluminescence measurements revealed that 5 μg/g CDDP inhibited

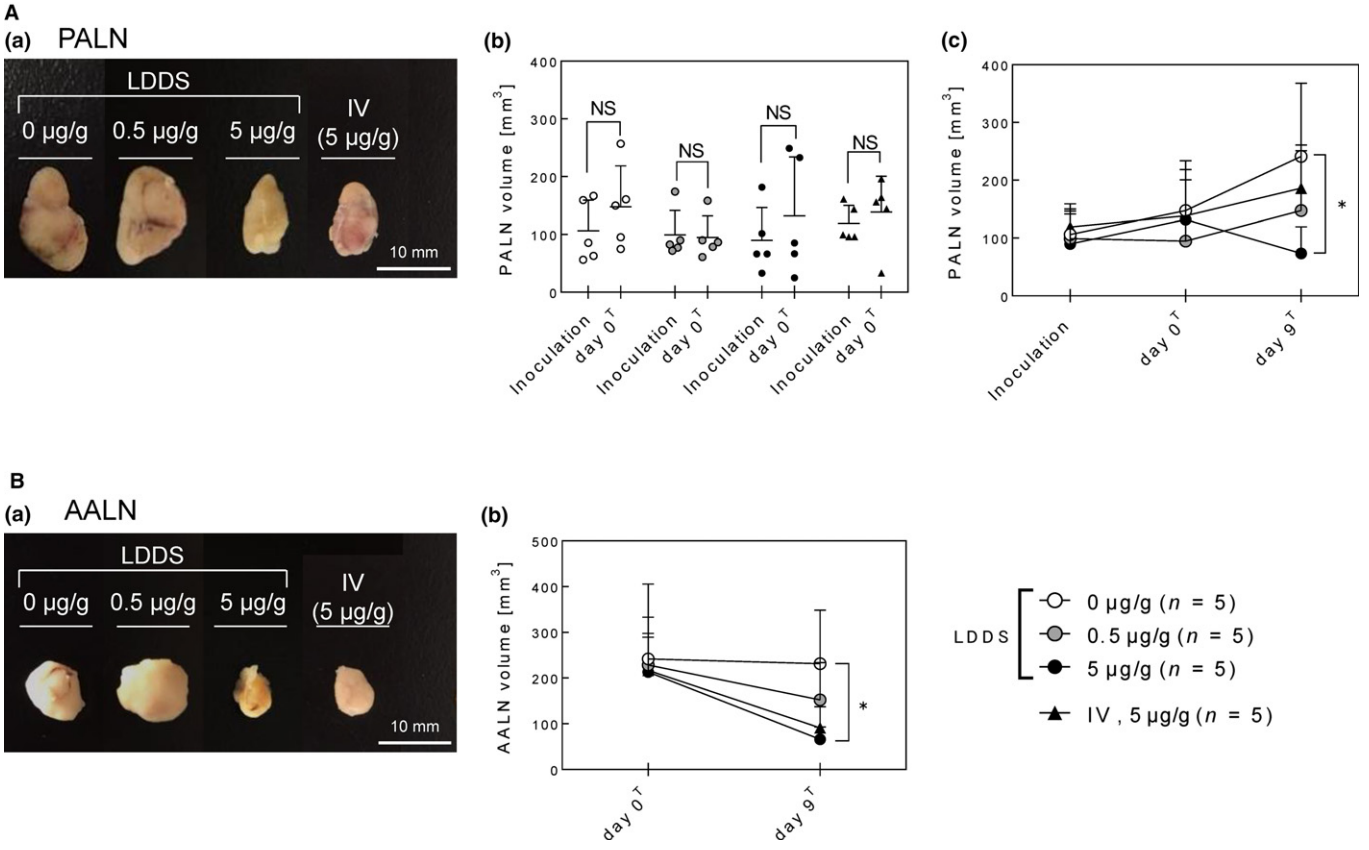

Fig. 3. Evaluation of proper axillary lymph node (PALN) and accessory axillary lymph node (AALN) volumes after treatment. (A) Changes in the volume of PALN measured using a high-frequency ultrasound (HFUS) imaging system. (a) Images of PALN at day 9^T after treatment. (b) Comparison of PALN volume between the inoculation day and day 0^T. In all groups, there were no significant increases in volume of PALN, indicating that metastatic PALN met the criteria for a false-negative metastatic lymph node (LN) (Wilcoxon signed rank test). (c) Effect of treatment on PALN volume. There were no significant differences in PALN volume between groups on the inoculation day and at day 0^T. In the control group, PALN volume increased about two-fold from the inoculation day to day 9^T. The lymphatic drug delivery system (LDDS) 5 μg/g cisplatin (CDDP) group exhibited an inhibition of PALN volume growth following treatment, with a statistically significant difference observed between the LDDS 0 μg/g CDDP and LDDS 5 μg/g CDDP groups (Kruskal-Wallis test: $^*P < 0.05$, 0 μg/g CDDP *vs* 5 μg/g CDDP). (B) Changes in volume of AALN measured using a HFUS imaging system. (a) Images of AALN at day 9^T after treatment. (b) Effect of treatment on AALN volume. There were no significant changes in AALN volume in the LDDS 0 μg/g CDDP and LDDS 0.5 μg/g CDDP groups. However, the LDDS 5 μg/g CDDP and i.v. injection (IV) (5 μg/g CDDP) groups showed a decrease in AALN volume after treatment. Statistically significant differences were observed between the LDDS 0 μg/g CDDP group and the LDDS 5 μg/g groups (Kruskal-Wallis test: $^*P < 0.05$, 0 μg/g CDDP *vs* 5 μg/g CDDP).

Table 1. Evaluation of toxicity 9 days after treatment

	LDDS			IV	
	0 μg/g (n = 4)	0.5 μg/g (n = 4)	0.5 μg/g (n = 5)	0.5 μg/g (n = 3)	Statistical significance
CRE (mg/dL)	0.10 ± 0.01	0.14 ± 0.02	0.13 ± 0.01	0.10 ± 0.01	NS
BUN (mg/dL)	27.98 ± 1.06	28.8 ± 0.89	35.66 ± 4.39	33.1 ± 4.88	NS
T-BIL (mg/dL)	0.05 ± 0.02	0.04 ± 0.02	0.072 ± 0.01	0.06 ± 0.02	NS
ALT (mg/dL)	52.25 ± 13.29	53 ± 18.53	59.4 ± 13.98	39.67 ± 1.20	NS
AST (mg/dL)	150.75 ± 31.38	120.5 ± 18.77	142.2 ± 24.70	146 ± 23.10	NS
Weight change (g)	1.60 ± 0.50	0.80 ± 0.90	−1.00 ± 0.50	0.00 ± 1.10	NS

ALT, alanine aminotransferase; AST, aspartate aminotransferase; BUN, blood urea nitrogen; Cre, creatinine; IV, intravenous group; LDDS, lymphatic drug delivery system NS, not significant; T-Bil, total bilirubin. Values are means ± SEM.

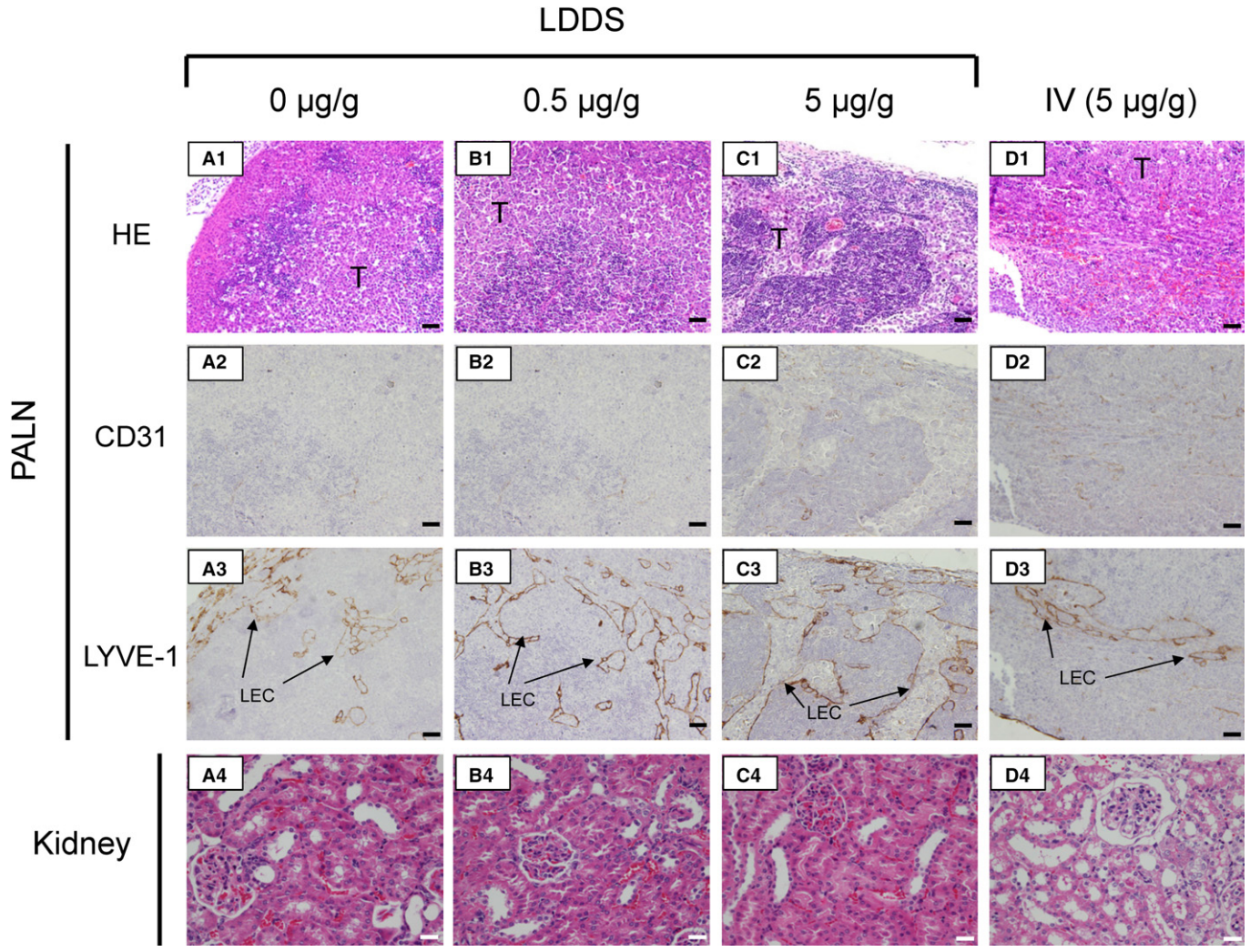

Fig. 4. Histological analysis. (A1–A4) lymphatic drug delivery system (LDDS) 0 μg/g cisplatin (CDDP) group. (B1–B4) LDDS 0.5 μg/g CDDP group. (C1–C4) LDDS 5 μg/g CDDP group. (D1–D4) i.v. injection (IV) (5 μg/g CDDP) group at day 9^{T}. (A1–A3, B1–B3, C1–C3, D1–D3) proper axillary lymph node (PALN) stained with H&E, anti-CD31 antibody or anti-LYVE-1 antibody. In the LDDS 0 μg/g CDDP (A3), LDDS 0.5 μg/g CDDP (B3) and IV (D3) groups, tumor had spread widely throughout the PALN despite treatment. In the LDDS 5 μg/g CDDP group (C3), tumor cells were observed only in lymphatic vessels. In all groups, lymphatic vessels had been expanded by tumor growth (A3, B3, C3, D3). LEC, lymphatic endothelial cells; T, tumor cells. Scale bar, 50 μm. (A4, B4, C4, D4) H&E staining of the kidney. Atrophy in the proximal convoluted tubules was observed in kidney sections from the IV group. Scale bar, 20 μm.

tumor growth when given by LDDS but not when given by i.v. injection (Fig. 2B,C). In addition, renal proximal tubular atrophy, a typical adverse effect of CDDP,[23] was detected after i.v. administration but not after administration through LDDS. Thus, LDDS may be a superior technique for drug delivery and retention in target LN, enhancing the response rate compared to systemic chemotherapy. When LDDS was used to deliver CDDP, volume of the drug injection site (LN

volume) tended to decrease; therefore, the total number of doses may be limited to one or two at most.

Giving 5 μg/g CDDP using LDDS significantly inhibited PALN tumor growth, but tumor cells were not completely eliminated (Fig. 4).

Proper axillary lymph node volume increased after IV administration of CDDP (Fig. 3Ab), and this treatment only slightly inhibited PALN tumor growth (Fig. 2Bb). Interestingly, the volume of the AALN (located upstream of the PALN) was greatly reduced by 5 μg/g CDDP, which was probably because of bone marrow suppression by CDDP. The reduction rate was almost the same for direct injection of CDDP into the AALN by LDDS. That is, LDDS has the potential to treat targeted LN effectively compared to systemic chemotherapy, with side-effects such as bone marrow suppression. The present study has demonstrated an antitumor effect of CDDP given with a LDDS on a false-negative metastatic LN and compared this effect with systemic i.v. administration of CDDP. Use of LDDS showed a notable advantage over i.v. administration in terms of molecular retention of drug in the target LN. In addition, CDDP administration with LDDS produced inhibition of tumor growth in LN without the serious adverse effects normally produced after i.v. injection of CDDP. LDDS shows great potential as an effective treatment for false-negative metastatic LN. In the present study, we supposed that CDDP would show similar flux/accumulation properties to ICG, as their molecular weights are similar. However, parameters such as size, surface charge, molecular weight, hydrophobicity and composition determine molecular retention in lymph nodes by LDDS. In addition, intranodal veins anastomose the vein running over the lymph node.[24] Thus, part of the drug injected into the lymph node flows into the vein. In LDDS, drug retention in lymph nodes and biodistribution in the whole body must be investigated. In addition, in future study, we intend to determine maximum tolerated dose, dose-limiting toxicity and to construct a dose–response curve to establish the most effective CDDP dose for completely treating tumor cells in metastatic LN.

Acknowledgments

This study was supported, in part, by JSPS KAKENHI Grant Numbers 26293425 (S.M.), 16K15816 (S.M.), and 17H00865 (T.K.). The authors thank T. Sato for technical assistance, and the Biomedical Research Core of Tohoku University Graduate School of Medicine for technical support.

Disclosure Statement

Authors declare no conflicts of interest for this article.

Abbreviations

AALN	accessory axillary lymph node
ALT	alanine aminotransferase
AST	aspartate aminotransferase
BUN	blood urea nitrogen
CDDP	cisplatin
Cre	creatinine
HFUS	high-frequency ultrasound
ICG	indocyanine green
LDDS	lymphatic drug delivery system
LN	lymph node
PALN	proper axillary lymph node
SiLN	subiliac lymph node
T-Bil	total bilirubin
VEGF	vascular endothelial growth factor

References

1 Alitalo A, Detmar M. Interaction of tumor cells and lymphatic vessels in cancer progression. *Oncogene* 2012; **31**: 4499–508.
2 Tanis PJ, Nieweg OE, Olmos RAV, Emiel J, Kroon BB. History of sentinel node and validation of the technique. *Breast Cancer Res* 2001; **3**: 1.
3 McAllaster JD, Cohen MS. Role of the lymphatics in cancer metastasis and chemotherapy applications. *Adv Drug Deliv Rev* 2011; **63**: 867–75.
4 Zhang Z, Helman JI. Li L-j. Lymphangiogenesis, lymphatic endothelial cells and lymphatic metastasis in head and neck cancer – a review of mechanisms. *Int J Oral Sci* 2010; **2**: 5.
5 Gipponi M, Canavese G, Lionetto R *et al.* The role of axillary lymph node dissection in breast cancer patients with sentinel lymph node micrometastases. *Eur J Surg Oncol* 2006; **32**: 143–7.
6 Giuliano AE, Hawes D, Ballman KV *et al.* Association of occult metastases in sentinel lymph nodes and bone marrow with survival among women with early-stage invasive breast cancer. *JAMA* 2011; **306**: 385–93.
7 Minchinton AI, Tannock IF. Drug penetration in solid tumours. *Nat Rev Cancer* 2006; **6**: 583–92.
8 Ryan GM, Kaminskas LM, Porter CJ. Nano-chemotherapeutics: maximising lymphatic drug exposure to improve the treatment of lymph-metastatic cancers. *J Control Release* 2014; **193**: 241–56.
9 Kodama T, Matsuki D, Tada A, Takeda K, Mori S. New concept for the prevention and treatment of metastatic lymph nodes using chemotherapy administered via the lymphatic network. *Sci Rep* 2016; **6**: 32506.
10 Shao L, Takeda K, Kato S, Mori S, Kodama T. Communication between lymphatic and venous systems in mice. *J Immunol Methods* 2015; **424**: 100–5.
11 Cho JK, Hyun SH, Choi N *et al.* Significance of lymph node metastasis in cancer dissemination of head and neck cancer. *Transl Oncol* 2015; **8**: 119–25.
12 Shao L, Mori S, Yagishita Y *et al.* Lymphatic mapping of mice with systemic lymphoproliferative disorder: usefulness as an inter-lymph node metastasis model of cancer. *J Immunol Methods* 2013; **389**: 69–78.
13 Ito K, Noro K, Yanagisawa Y *et al.* High-accuracy ultrasound contrast agent detection method for diagnostic ultrasound imaging systems. *Ultrasound Med Biol* 2015; **41**: 3120–30.
14 Miura Y, Mikada M, Ouchi T *et al.* Early diagnosis of lymph node metastasis: importance of intranodal pressures. *Cancer Sci* 2016; **107**: 224–32.
15 Kato S, Shirai Y, Kanzaki H, Sakamoto M, Mori S, Kodama T. Delivery of molecules to the lymph node via lymphatic vessels using ultrasound and nano/microbubbles. *Ultrasound Med Biol* 2015; **41**: 1411–21.
16 Sato T, Mori S, Arai Y, Kodama T. The combination of intralymphatic chemotherapy with ultrasound and nano-/microbubbles is efficient in the treatment of experimental tumors in mouse lymph nodes. *Ultrasound Med Biol* 2014; **40**: 1237–49.
17 Sato T, Mori S, Sakamoto M, Arai Y, Kodama T. Direct delivery of a cytotoxic anticancer agent into the metastatic lymph node using nano/microbubbles and ultrasound. *PLoS One* 2015; **10**: e0123619.
18 Kodama T, Hatakeyama Y, Kato S, Mori S. Visualization of fluid drainage pathways in lymphatic vessels and lymph nodes using a mouse model to test a lymphatic drug delivery system. *Biomed Opt Express* 2015; **6**: 124–34.
19 Li L, Mori S, Kodama M, Sakamoto M, Takahashi S, Kodama T. Enhanced sonographic imaging to diagnose lymph node metastasis: importance of blood vessel volume and density. *Cancer Res* 2013; **73**: 2082–92.
20 Li L, Mori S, Sakamoto M, Takahashi S, Kodama T. Mouse model of lymph node metastasis via afferent lymphatic vessels for development of imaging modalities. *PLoS One* 2013; **8**: e55797.
21 Kato S, Mori S, Kodama T. A novel treatment method for lymph node metastasis using a lymphatic drug delivery system with nano/microbubbles and ultrasound. *J Cancer* 2015; **6**: 1282–94.
22 Shao L, Ouchi T, Sakamoto M, Mori S, Kodama T. Activation of latent metastases in the lung after resection of a metastatic lymph node in a lymph node metastasis mouse model. *Biochem Biophys Res Commun* 2015; **460**: 543–8.
23 Pinzani V, Bressolle F, Haug IJ, Galtier M, Blayac JP, Balmès P. Cisplatin-induced renal toxicity and toxicity-modulating strategies: a review. *Cancer Chemother Pharmacol* 1994; **35**: 1–9.
24 Takeda K, Mori S, Kodama T. Study of fluid dynamics reveals direct communications between lymphatic vessels and venous blood vessels at lymph nodes of mice. *J Immunol Methods* 2017; **445**: 1–9.